CFD Letters 14, Issue 11 (2022) 88-101

CFD Letters

Journal homepage:
https://semarakilmu.com.my/journals/index.php/CFD_Letters/index
ISSN: 2180-1363

Magnetohydrodynamics Ag-Fe_3O_4-Ethylene Glycol Hybrid Nanofluid Flow and Heat Transfer with Thermal Radiation

Yap Bing Kho[1], Rahimah Jusoh[1,*], Mohd Zuki Salleh[1], Mohd Hisyam Ariff[2], Nooraini Zainuddin[3]

[1] Centre for Mathematical Sciences, Universiti Malaysia Pahang, 26300 Gambang, Kuantan, Pahang, Malaysia
[2] Faculty of Electrical & Electronics Engineering Technology, Universiti Malaysia Pahang, 26600 Pekan, Pahang, Malaysia
[3] Department of Fundamental & Applied Sciences, Universiti Teknologi PETRONAS, 32610 Bandar Seri Iskandar, Perak, Malaysia

ARTICLE INFO

Article history:
Received 25 July 2022
Received in revised form 5 September 2022
Accepted 7 September 2022
Available online 10 November 2022

Keywords:
Hybrid nanofluid; magnetohydrodynamic; thermal radiation; stability analysis

ABSTRACT

The potential of hybrid nanofluid as an alternative heat transfer fluid is undoubted and the insightful research on enhancing its thermal conductivity is crucial. This study accentuates the influence of magnetic field and thermal radiation on the ethylene glycol base hybrid nanofluid with a combination of argentum and magnetite nanoparticles. The mathematical equations of the hybrid nanofluid model are derived with the suitable similarity transformations and then solved numerically with the execution of bvp4c codes in Matlab software. Graphical results show that an upsurge in magnetic parameter reduces the momentum boundary layer thickness while the higher thermal radiation enlarges the thermal boundary layer thickness. The effects of suction and nanoparticles concentration are also presented graphically. Stability analysis reveals that the first solution obtained in this study is stable, and conversely, the second solution is not.

1. Introduction

Nanotechnology has piqued the interest of numerous academics, who have lately begun to use nanofluids in both experimental and theoretical studies. The growing interest in nanofluids in recent years stems from the discovery that employing ordinary fluid as a heat transfer medium has limitations. Choi and Eastman [1] theoretically established that adding nanoparticles stimulates heat conductivity. Nanofluid has extensive applications in the industrial, technical, and biological fields such as drug delivery, microchip cooling, hybrid-powered engines, cancer therapies, geothermal power extraction and industrial cooling. Latib and Kamaruzaman [2] demonstrated that nanofluid can be the ideal substitute for water as the coolant for rotating detonation engines. Researchers have recently concentrated on the new class of nanofluids known as hybrid nanofluids, which entail the inclusion of two or more nanoparticles to improve the heat transfer performance of nanofluids. Esfe *et al.,* [3] conducted experimental work on argentum-magnesium oxide/water hybrid nanofluid and found that when the nanoparticle volume fraction was raised, the dynamic viscosity and thermal

* *Corresponding author.*
E-mail address: rahimahj@ump.edu.my *(Rahimah Jusoh)*

https://doi.org/10.37934/cfdl.14.11.88101

conductivity of the nanofluid escalated. A year later, Harandi *et al*., [4] considered ethylene glycol as the base fluid with the combination of the magnetite nanoparticles and multi-wall carbon nanotube to examine the heat conductivity of this hybrid nanofluid. They reported 30% enhancement of thermal conductivity of nanofluid with 2.3% solid volume fraction. The non-isothermal hybrid nanofluid was the subject of investigation by Jahan *et al*., [5], and they noticed that an increase in viscous dissipation is seen to dramatically boost temperatures across the boundary layer regime. Hybridization of nanoparticles also can improve the fluid thermal conductivity and produce higher stability [6,7]. Moreover, hybrid nanofluid can be utilised in the air conditioning system where it functions as the refrigerant and prevents overheating [6]. One of the elements that can be considered in exploring the flow of hybrid nanofluid is magnetohydrodynamic (MHD). Magnetohydrodynamic flow has been the subject of a lot of research in the past, which involving the study of the magnetic characteristics and behaviour of electro-conductive fluids in the presence of a magnetic field. By coupling fluid flow with magnetic fields, magnetohydrodynamic participation in boundary layer flow regulates the fluid flow. In addition, the phenomenon of magnetohydrodynamics also significant in metallurgy process, chemical catalytic reactors, astrophysics and production of float glass [9]. Latterly, Ezhil *et al*., [10] considered magnetic field in the Cu-Fe_3O_4/ ethylene glycol hybrid nanofluid and discovered that as the presence of the magnetic field gets stronger, the nanofluid velocity declined.

Besides the magnetic parameter, the influence of thermal radiation has also become a prevailing topic among the researchers since it has a significant impact on heat transfer on surfaces. Thermal radiation is also used as a source of alternative energy. It radiated energy onto the surface and subsequently raising the surface temperature in the process. Sreedevi *et al*., [11] considered thermal radiation in the unsteady hybrid nanofluid flow and found that greater radiative heat transfer led to the thicker thermal boundary layer. Motivated by the above-mentioned investigations, the potential of hybrid nanofluid as a superior heat transfer medium should not be overlooked. In this study, the hybrid nanofluid is modelled with the combination of the argentum Ag nanoparticles (which also known as silver) and magnetite Fe_3O_4 (iron oxide) nanoparticles with ethylene glycol $C_2H_6O_2$ as the base fluid. In addition, the effects of magnetic field and thermal radiation are also taken into account.

2. Problem Formulation

The Ag-Fe_3O_4 hybrid nanofluid model is investigated in the rectangular coordinate frame with the stretched/shrunk surface that parallel to *x*-axis and *y*-axis is orthogonal to the surface. For a better understanding of the flow configuration, Figure 1 portrays the coordinate system and the flow diagram of this model. The flow is affected by the permeable surface with the velocity $u = \lambda u_w\left(x\right) = \lambda ax$ for stretching surface $\left(\lambda > 0\right)$ and shrinking surface $\left(\lambda < 0\right)$, whereas the mass flux velocity is represented by v_w. Besides, the magnetic field B_0 is orthogonally imposed to the stretching/shrinking surface.

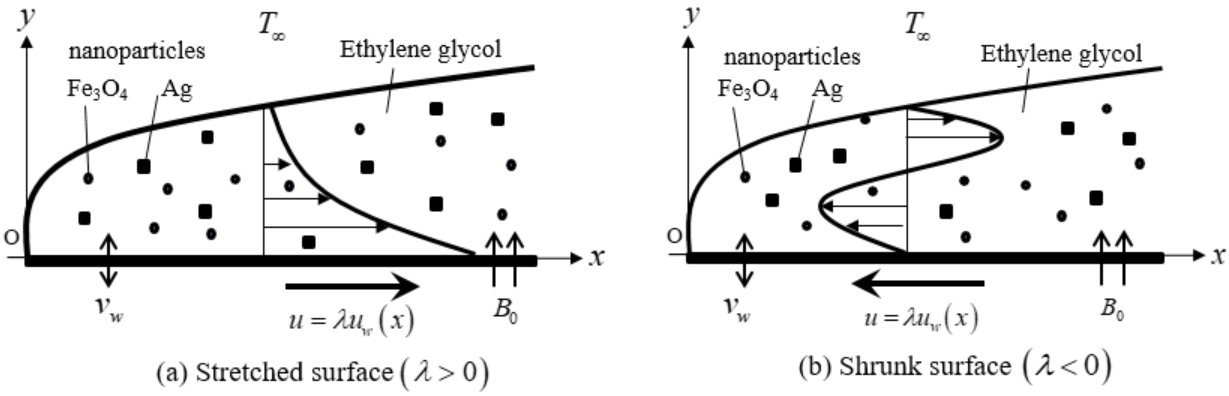

Fig. 1. Coordinate system and flow diagram

The derivation of the hybrid nanofluid flow equations are adopted from the two-dimensional Navier-Stokes equation which including the continuity equation reflecting viscous incompressible flow, momentum equation in terms of *u* and *v* components and the energy equation as follows:

$$\frac{\partial u}{\partial x}+\frac{\partial v}{\partial y}=0, \tag{1}$$

$$u\frac{\partial u}{\partial x}+v\frac{\partial u}{\partial y}=\frac{\mu_{hnf}}{\rho_{hnf}}\frac{\partial^2 u}{\partial y^2}-\frac{\sigma_{hnf}B_0^{\,2}}{\rho_{hnf}}u, \tag{2}$$

$$u\frac{\partial T}{\partial x}+v\frac{\partial T}{\partial y}=\alpha_{hnf}\frac{\partial^2 T}{\partial y^2}-\frac{1}{\left(\rho C_p\right)_{hnf}}\frac{\partial q_r}{\partial y}. \tag{3}$$

The extra term for magnetic field B_0 is included in the momentum equation and the radiative heat flux q_r is encompassed in the energy equation. These governing equations are relying to the respective boundary conditions

$$\begin{array}{llll} u=\lambda u_w(x) & v=-v_w & T=T_w & \text{at} \quad y=0 \\ u\to 0, & T\to T_\infty & & \text{as} \quad y\to\infty \end{array}, \tag{4}$$

In the boundary condition, the surface temperature is symbolized as T_w whereas T_∞ is the uniform temperature of the ambient hybrid nanofluid. Additionally, mathematical equations of the hybrid nanofluid model involve the heat capacity parameter, thermal conductivity, density, electrical conductivity, dynamic viscosity as well as thermal diffusivity which are represented by $(\rho C_p)_{hnf}$, k_{hnf}, ρ_{hnf}, σ_{hnf}, μ_{hnf} and α_{hnf}, respectively. The formulations of the hybrid nanofluid properties are listed in Table 1. Subscript *s*1 in this table represents the argentum nanoparticles while *s*2 represents the magnetite nanoparticles. The base fluid (ethylene glycol) is denoted by subscript *f*, nanofluid by *nf* and hybrid nanofluid by *hnf*. Then, by following Takabi and Salehi [12], the overall volume concentration of argentum and magnetite dispersed in hybrid nanofluid is formulated as $\phi_{hnf}=\phi_1+\phi_2$ since the correlation is practical and based on physical assumptions. As a reference, the thermophysical attributes of the ethylene glycol and nanoparticles are presented in Table 2.

Table 1
Formulations of hybrid nanofluid properties [12–14]

Properties	Nanofluid	Hybrid nanofluid
Density	$\rho_{nf}=(1-\phi_1)\rho_f+\phi_1\rho_s$	$\rho_{hnf}=(1-\phi_{hnf})\rho_f+\phi_1\rho_{s1}+\phi_2\rho_{s2}$
Heat capacity	$(\rho C_p)_{nf}=(1-\phi_1)(\rho C_p)_f+\phi_1(\rho C_p)_s$	$(\rho C_p)_{hnf}=(1-\phi_{hnf})(\rho C_p)_f+\phi_1(\rho C_p)_{s1}+\phi_2(\rho C_p)_{s2}$
Dynamic viscosity	$\mu_{nf}=\dfrac{\mu_f}{(1-\phi_1)^{2.5}}$	$\dfrac{\mu_{hnf}}{\mu_f}=\dfrac{1}{(1-\phi_{hnf})^{2.5}}$
Thermal Conductivity	$k_{nf}=\dfrac{k_s+2k_f-2\phi_1(k_f-k_s)}{k_s+2k_f+\phi_1(k_f-k_s)}\times k_f$	$\dfrac{k_{hnf}}{k_f}=\dfrac{\left(\dfrac{\phi_1k_{s1}+\phi_2k_{s2}}{\phi_{hnf}}\right)+2k_f+2(\phi_1k_{s1}+\phi_2k_{s2})-2\phi_{hnf}k_f}{\left(\dfrac{\phi_1k_{s1}+\phi_2k_{s2}}{\phi_{hnf}}\right)+2k_f-(\phi_1k_{s1}+\phi_2k_{s2})+\phi_{hnf}k_f}$
Electrical Conductivity	$\dfrac{\sigma_{nf}}{\sigma_f}=1+\dfrac{3\left(\dfrac{\sigma_s}{\sigma_f}-1\right)\phi_1}{\left(\dfrac{\sigma_s}{\sigma_f}+2\right)-\left(\dfrac{\sigma_s}{\sigma_f}-1\right)\phi_1}$	$\dfrac{\sigma_{hnf}}{\sigma_f}=1+\dfrac{3\left(\dfrac{\phi_1\sigma_{s1}+\phi_2\sigma_{s2}}{\sigma_f}-\phi_{hnf}\right)}{\left(\dfrac{\phi_1\sigma_{s1}+\phi_2\sigma_{s2}}{\phi_{hnf}\sigma_f}+2\right)-\left(\dfrac{\phi_1\sigma_{s1}+\phi_2\sigma_{s2}}{\sigma_f}-\phi_{hnf}\right)}$

Table 2
Thermophysical attributes of the ethylene glycol and nanoparticles [10,15–17]

Properties	$\rho\left(kgm^{-3}\right)$	$C_p\left(Jkg^{-1}K^{-1}\right)$	$k\left(Wm^{-1}K^{-1}\right)$	$\sigma(s/m)$
Ag	10500	235	429	6.3×10^{7}
Fe_3O_4	5180	670	9.7	12.7
$C_2H_6O_2$	1115	2430	0.253	1.07×10^{-4}

The following similarity transformations are used to simplify the governing Eqs. (1)-(3), which relate to the boundary conditions in Eq. (4)

$$u=a\,xf'(\eta),\quad v=-\sqrt{a\nu_f}\,f(\eta),\quad \eta=y\sqrt{\frac{a}{\nu_f}},\quad \theta(\eta)=\frac{T-T_\infty}{T_w-T_\infty}. \tag{5}$$

Eq. (1) is now automatically satisfied. Subsequently, Eq. (2) and Eq. (3) are abridged to the following ordinary differential equations:

$$\frac{\mu_{hnf}/\mu_f}{\rho_{hnf}/\rho_f}f'''+ff''-f'^2-\frac{\sigma_{hnf}/\sigma_f}{\rho_{hnf}/\rho_f}Mf'=0, \tag{6}$$

$$\frac{k_{hnf}/k_f+Rd}{(\rho C_p)_{hnf}/(\rho C_p)_f}\theta''+\Pr f\theta'=0, \tag{7}$$

depending on the boundary conditions

$$f(0)=s,\quad f'(0)=\lambda \quad \theta(0)=1,\quad f'(\infty)\to 0,\quad \theta(\infty)\to 0. \tag{8}$$

Here, *s* is the mass flux parameter and, in this study, we consider positive values of *s* for suction. Meanwhile, *M* is the magnetic number, *Rd* indicates the thermal radiation and *Pr* denotes the Prandtl number which are formulated as

$$\Pr=\frac{\nu_f\left(\rho C_p\right)_f}{k_f},\quad s=\frac{v_w}{\sqrt{a\nu_f}},\quad M=\frac{\sigma_f B_0^{\,2}}{\rho_f a},\qquad Rd=\frac{16\sigma^* T_\infty^{\,3}}{3k^* k_f} \tag{9}$$

The heat flux from the sheet q_w, the Nusselt number Nu_x and the skin friction coefficients C_f are defined as (Yushkun *et al.*, [18])

$$C_f=\frac{\mu_{hnf}}{\rho_f u_w^2}\left(\frac{\partial u}{\partial y}\right)_{y=0},\qquad Nu_x=\frac{x q_w}{k_f\left(T_w-T_\infty\right)},\qquad q_w=-k_{hnf}\left(\frac{\partial T}{\partial y}\right)_{y=0}+\left(q_r\right)_{y=0}. \tag{10}$$

The radiative heat flux q_r is indicated by

$$q_r=-\frac{4\sigma^*}{3k^*}\frac{\partial T^4}{\partial y}=-\frac{16\sigma^* T^3}{3k^*}\frac{\partial T}{\partial y} \tag{11}$$

using the Rosseland approximations. Then, we get the following Eq. (12) by applying the similarity transformations in Eq. (5) into Eq. (10) and Eq. (11)

$$\mathrm{Re}_x^{\frac{1}{2}} C_f=\frac{\mu_{hnf}}{\mu_f}f''(0),\qquad \sqrt{1/\mathrm{Re}_x}\,Nu_x=-\left(\frac{k_{hnf}}{k_f}+Rd\right)\theta'(0) \tag{12}$$

where $\mathrm{Re}_x=\dfrac{u_w x}{\nu_f}$ represents the local Reynolds number.

3. Stability Analysis

It is crucial to do a stability analysis to establish whether the solutions are physically feasible. First, as proposed by Merkin [19], the unsteady case for Eq. (2)-(4) must be examined, which can be written as

$$\frac{\partial u}{\partial t}+u\frac{\partial u}{\partial x}+v\frac{\partial u}{\partial y}=\frac{\mu_{hnf}}{\rho_{hnf}}\frac{\partial^2 u}{\partial y^2}-\frac{\sigma_{hnf}B_0^{\,2}}{\rho_{hnf}}u, \tag{13}$$

$$\frac{\partial T}{\partial t}+u\frac{\partial T}{\partial x}+v\frac{\partial T}{\partial y}=\alpha_{hnf}\frac{\partial^2 T}{\partial y^2}-\frac{1}{\left(\rho C_p\right)_{hnf}}\frac{\partial q_r}{\partial y}, \tag{14}$$

where *t* demonstrating the time. Weidman *et al.*, [20] mentioned that stability analysis requires the introduction of a new dimensionless time variable τ. As a result, the new similarity transformations are

$$u = a\,x\,\frac{\partial f}{\partial \eta}(\eta,\tau), \qquad v = -\sqrt{a\nu_f}\, f(\eta,\tau),$$
$$\theta(\eta,\tau) = \frac{T - T_\infty}{T_w - T_\infty}, \qquad \eta = \sqrt{\frac{a}{\nu_f}}\, y, \qquad \tau = at. \tag{15}$$

We obtain the following equations by substituting similarity variables in Eq. (15) into Eq. (13) and Eq. (4):

$$\frac{\mu_{hnf}/\mu_f}{\rho_{hnf}/\rho_f}\frac{\partial^3 f}{\partial \eta^3} + f\frac{\partial^2 f}{\partial \eta^2} - \left(\frac{\partial f}{\partial \eta}\right)^2 - \frac{\sigma_{hnf}/\sigma_f}{\rho_{hnf}/\rho_f} M\frac{\partial f}{\partial \eta} - \frac{\partial^2 f}{\partial \eta \partial \tau} = 0, \tag{16}$$
$$\frac{1}{\Pr}\frac{k_{hnf}/k_f + Rd}{\left(\rho C_p\right)_{hnf}/\left(\rho C_p\right)_f}\frac{\partial^2 \theta}{\partial \eta^2} + f\frac{\partial \theta}{\partial \eta} - \frac{\partial \theta}{\partial \tau} = 0, \tag{17}$$

accompanied by the boundary conditions

$$f(0,\tau) = s, \quad \frac{\partial f}{\partial \eta}(0,\tau) = \lambda, \quad \theta(0,\tau) = 1, \quad \frac{\partial f}{\partial \eta}(\infty,\tau) \to 0, \quad \theta(\infty,\tau) \to 0. \tag{18}$$

The stability behaviour may be assessed by perturbing the fundamental flow $f = f_0(\eta)$ and $\theta = \theta_0(\eta)$ as proposed by Weidman *et al.*, [20] with the following functions

$$f(\eta,\tau) = f_0(\eta) + e^{-\gamma\tau} F(\eta), \qquad \theta(\eta,\tau) = \theta_0(\eta) + e^{-\gamma\tau} H(\eta), \tag{19}$$

where γ is an unspecified eigenvalue parameter, and $F(\eta)$ and $H(\eta)$ are relatively small to $f_0(\eta)$ and $\theta_0(\eta)$. The solution for the eigenvalue problems in Eq. (16)-(18) results in an infinite set of $\gamma_1 < \gamma_2 < \gamma_3 \ldots$, and γ_1 is the minimum eigenvalue. If γ_1 is negative in this scenario, there is an initial increase in disturbances, indicating that the flow is unstable. The flow, on the other hand, is considered to be stable if γ_1 is positive and there is an initial decline in disturbances. Substituting Eq. (19) into Eq. (16)-(18) yields the following linearized equations:

$$\frac{\mu_{hnf}/\mu_f}{\rho_{hnf}/\rho_f} F''' + f_0 F'' + F f_0'' - 2 f_0' F' - \frac{\sigma_{hnf}/\sigma_f}{\rho_{hnf}/\rho_f} M F' + \gamma F' = 0, \tag{20}$$
$$\frac{1}{\Pr}\frac{k_{hnf}/k_f + Rd}{\left(\rho C_p\right)_{hnf}/\left(\rho C_p\right)_f} G'' + f_0 G' + F\theta_0' + \gamma G = 0, \tag{21}$$

subject to

$$F(0) = 0, \quad F'(0) = 0, \quad G(0) = 0, \quad F'(\infty) \to 0, \quad G(\infty) \to 0. \tag{22}$$

The range of potential eigenvalues can be generated by loosening a boundary condition at $\eta \to \infty$ [21]. Accordingly, the boundary condition $F'(\infty) \to 0$ was loosened, and the system of Eq. (20)-(22) was solved using the stabilizing boundary condition $F''(0) = 1$.

4. Results and Discussion

To offer a physical observation of the flow problem, numerical simulations have been done thoroughly utilizing the built-in bvp4c function in Matlab programme. The current findings of the local Nusselt number are compared to prior research by Mukhopadhyay [22] to verify the correctness and validity of the present study. Mukhopadhyay [22] utilized the shooting technique to obtain the results for a certain value of parameters. The comparisons, as shown in Table 1, demonstrate great agreement, indicating that the bvp4c function used in the present study is legitimate. Moreover, Table 3 also exhibits an increment in the local Nusselt number as the value of Prandtl number *Pr* increasing but slightly decreases as the thermal radiation and magnetic parameter rises. These results elucidate that an increase in the magnetic field and thermal radiation cause a reduction in the process of heat transfer.

Table 3
Comparison of $-\theta'(0)$ for various values of *Pr*, *Rd* and *M* when $\phi_1 = \phi_2 = S = 0$ and $\lambda = 1$.

Pr	*Rd*	*M*	Mukhopadhyay [22]	Present Results
1	0	0	0.9547	0.954782709
5	0	0	2.5001	2.500131408
10	0	0	3.6603	3.660371730
1	0	1	0.8610	0.861094745
1	1	0	0.5311	0.531239860
1	1	1	0.4503	0.451162010
2	0.5	0	1.0734	1.073518899
3	0.5	0	1.3807	1.380752049

The graphical analysis of the boundary layer flow of argentum-magnetite (Ag-Fe_3O_4) hybrid nanofluid flow and heat transfer is conducted. Since the base fluid is ethylene glycol ($C_2H_6O_2$), thus Prandtl number used in this study is 24.4. The impacts of several governing dimensionless parameters, such as the magnetic parameter, thermal radiation parameter, suction parameter, and nanoparticle concentration on the velocity as well as temperature profiles are determined and depicted in Figures 2-9.

The performance of the magnetic parameter on the velocity profile is shown in Figure 2, which demonstrates a decrease in the thickness of the momentum boundary layer for the first solution within the specified values. It is noticed that when the magnetic parameter's value increases, the thickness of the boundary layer thins. The Lorentz force is increased by the high magnetic field inside the boundary layer, which greatly opposes the flow in the opposite direction.

Figure 3 shows the influence of the radiation parameter on the temperature profiles, and it shows that the thickness of the thermal boundary layer for both solutions increases. Generally, increasing the value of the radiation parameter indicates more radiative heat energy will be emitted from the hybrid nanofluid flow, and subsequently causing a rise in the temperature distribution profile. The same pattern of graph also had been obtained by Thirupathi *et al.,* [23] where they concluded that the rising of thermal radiation enhanced the fluid’s energy distribution.

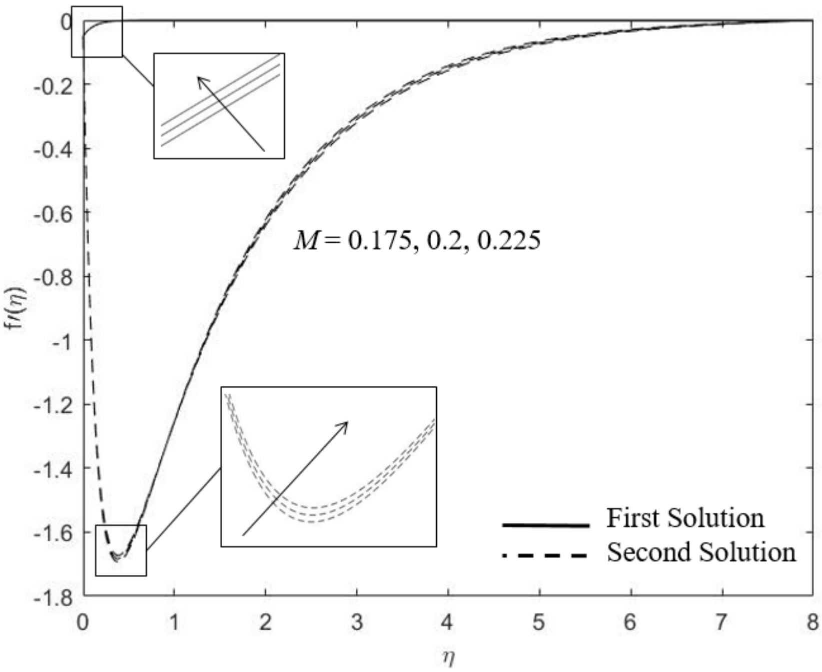

Fig. 2. Trends in $f'(\eta)$ for various *M* values

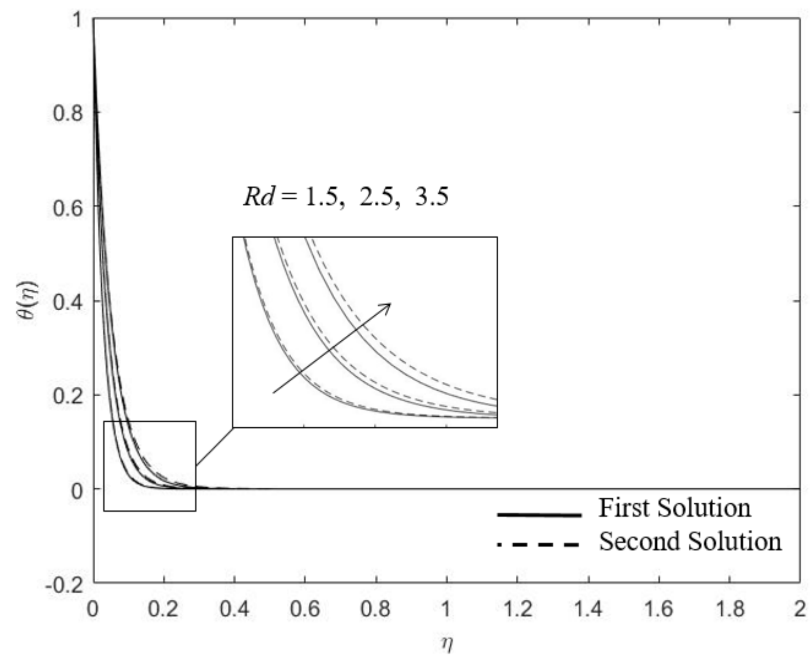

Fig. 3. Trends in $\theta(\eta)$ for various *Rd* values

Figure 4 demonstrates that when suction increases, the velocity gradient at the surface increases, implying an increase in wall shear stress. This will diminish the thickness of the momentum boundary layer indirectly. At the same time, increased suction results in a decrease in the temperature distribution profile, as seen in Figure 5. Subsequently, the thinning thermal boundary layer thickness will stimulate the process of heat transfer.

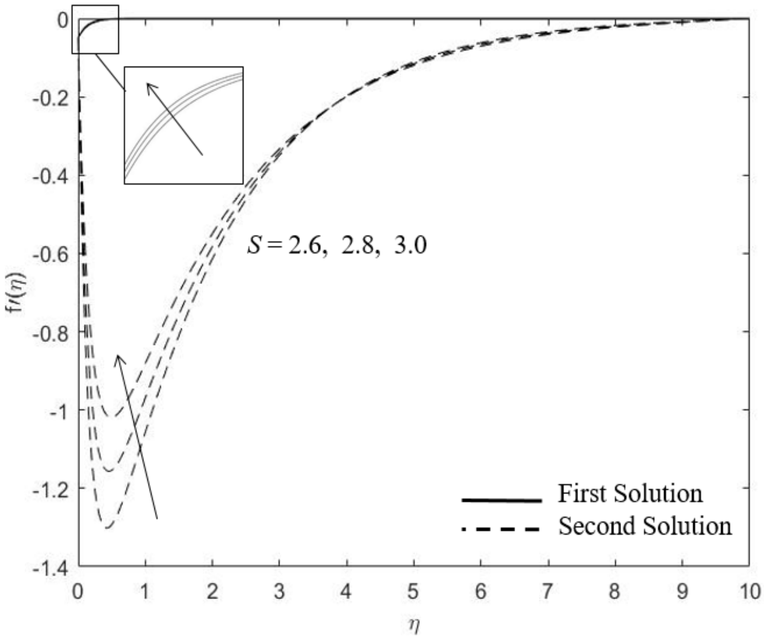

Fig. 4. Trends in $f'(\eta)$ for various *S* values

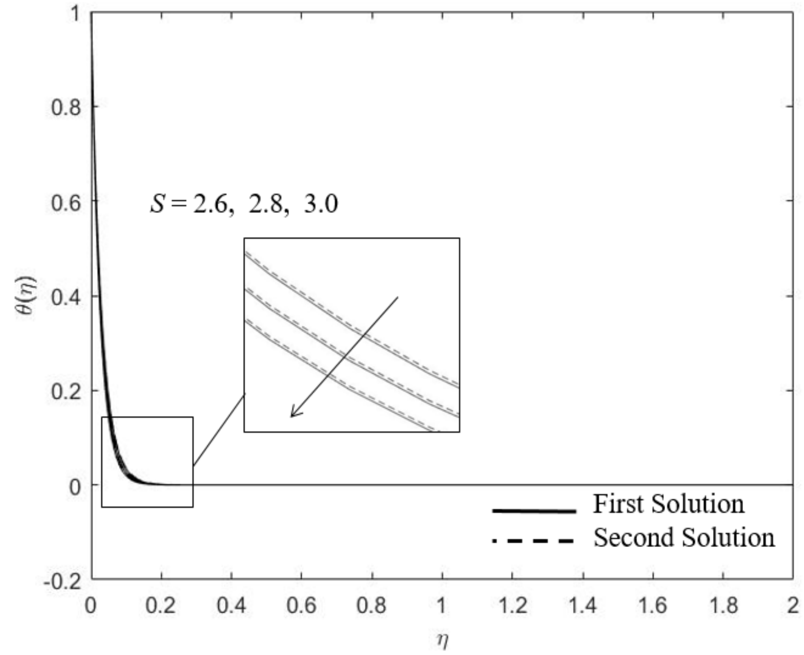

Fig. 5. Trends in $\theta(\eta)$ for various *S* values

Figure 6 delineates the effect of argentum Ag nanoparticles volume fraction ϕ_1 on the velocity distribution profile. The higher volume fraction of argentum increases the velocity for the first solution but there is an opposite behaviour for the second solution. Meanwhile, the higher concentration of Ag nanoparticles causes the decrement in temperature distribution profile for dual solutions as shown in Figure 7. In contrast, Figure 8 illustrates the influence of magnetite (Fe_3O_4) nanoparticles concentration ϕ_2 on the velocity distribution profile. The first solution shows the decrement of the velocity, but the second solution shows the improvement of it. Besides, magnetite nanoparticles concentration causes the increment in temperature distribution profile for dual solutions as portrayed in Figure 9. Conclusively, variations of argentum nanoparticles concentration give different impacts to the velocity and temperature profile as compared to the variations in the magnetite nanoparticles. This is most probably owing to the fact that the reactivity of magnetite or iron oxide is higher than the argentum.

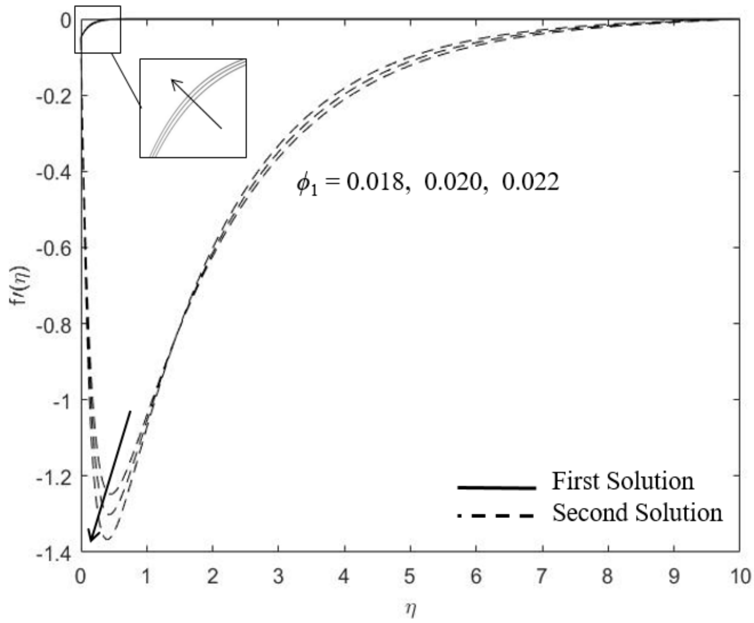

Fig. 6. Ag concentration's effects on $f'(\eta)$

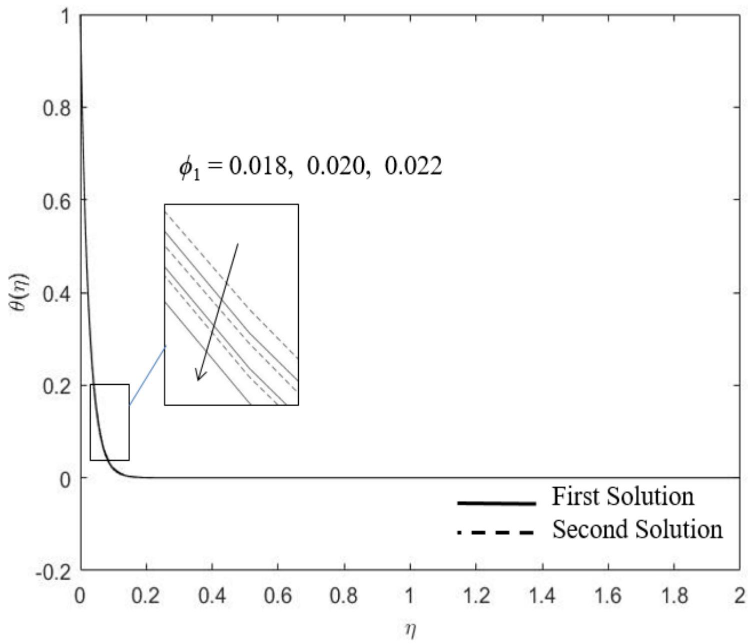

Fig. 7. Ag concentration's effects on $\theta(\eta)$

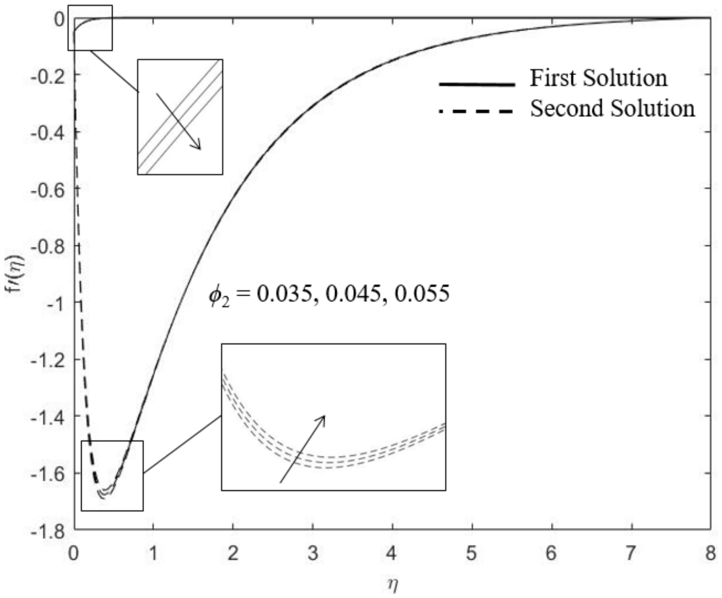

Fig. 8. Fe_3O_4 concentration's effects on $f'(\eta)$

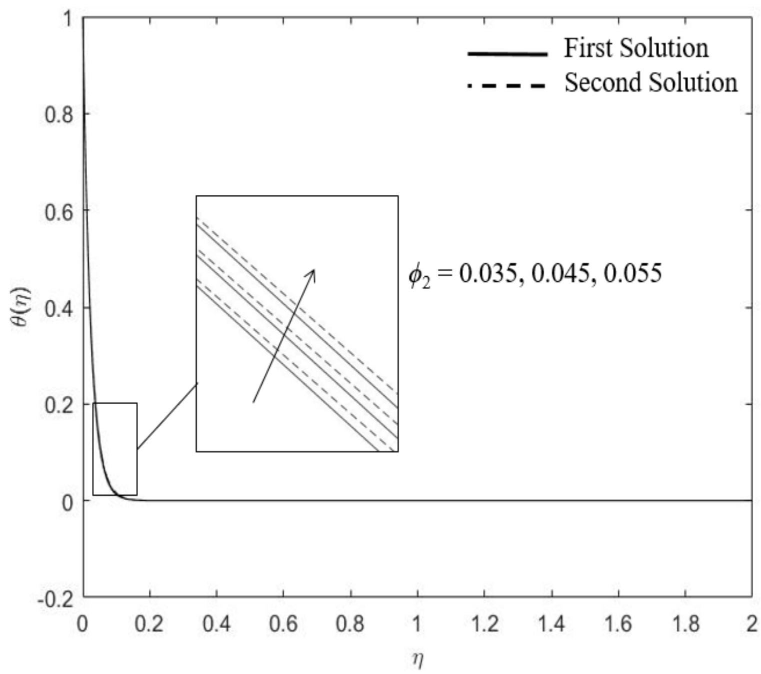

Fig. 9. Fe_3O_4 concentration's effects on $\theta(\eta)$

Figure 10 illustrates the variation of the Nusselt number $\sqrt{1/\mathrm{Re}_x}Nu_x$ in response to a change in the values of thermal radiation parameter *Rd*. It is obviously seen that the results of the Nusselt number declines as *Rd* increases. Physically, higher thermal radiation contributes to the higher temperature of the hybrid nanofluid and enhances the thermal boundary layer thickness because the surface heat flux increases under the impact of thermal radiation. Therefore, this circumstance will reduce the rate of heat transfer.

To determine the viability of the first and second options, stability analysis is necessary. As illustrated in Figure 11, it was accomplished by solving the eigenvalue problems in Eq. (20)-(22) and calculating the lowest eigenvalue γ_1. Positive values of γ_1 cause decay, meaning that the initial solution has a stabilizing feature. Negative values of γ_1, on the other hand, imply the expansion of disturbances in the second solution. Therefore, the first solution is clearly stable, but the second solution is unstable, as seen in Figure 11.

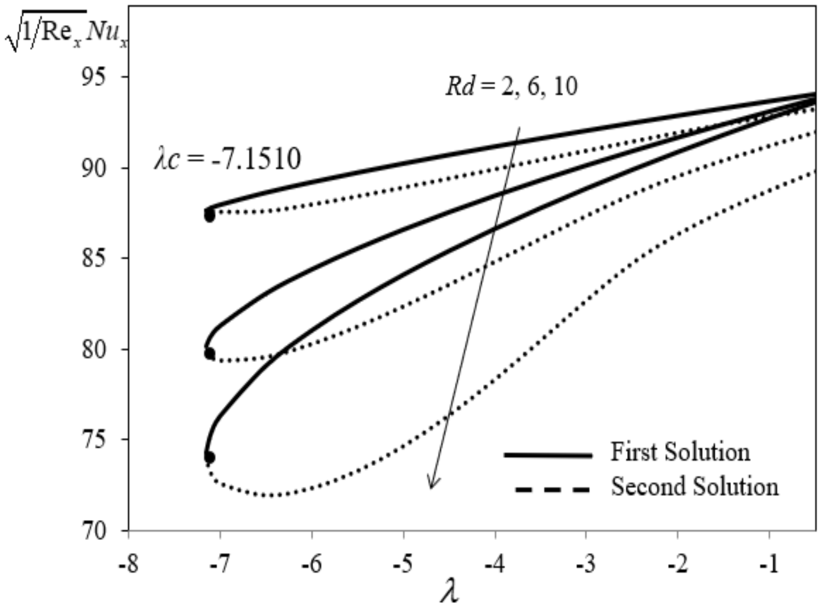

Fig. 10. Variations of the Nusselt number for some values of *Rd*

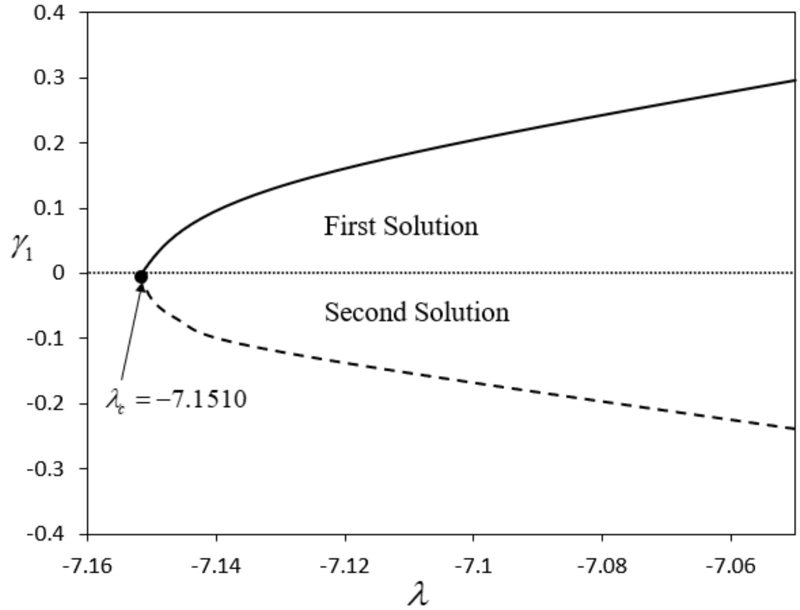

Fig. 11. Variations of γ_1 with λ

5. Conclusions

The mathematical modelling of argentum-magnetite (Ag-Fe_3O_4) hybrid nanofluid with the base fluid of ethylene glycol was examined. The analysis of the physical insight heat transfer with thermal radiation and magnetic field was examined. Physical insight analysis of the hybrid nanofluid model was devoted on the flow and heat transfer rate with the inclusion of magnetic field and thermal radiation. The velocity distribution profile increased by the presence of magnetic parameter and suction, which led to diminution of the momentum boundary layer thickness for the first solution. For both solutions, the temperature profile revealed a decrease in Ag nanoparticle volume fraction, whereas the Fe_3O_4 nanoparticle volume fraction had the opposite trend. The existence of thermal radiation increased the surface heat flux and subsequently deteriorated the process of heat transfer. Finally, stability analysis of both solutions proved the feasibility of the first solutions with the positive eigenvalue. In future, this study can be extended by considering the other physical configurations and governing parameters.

Acknowledgement
The authors would like to express their gratitude to Universiti Malaysia Pahang for funding this work with research funds (RDU1903143, RDU213201 and RDU223202).

References

[1] Choi, S. US, and Jeffrey A. Eastman. *Enhancing thermal conductivity of fluids with nanoparticles*. No. ANL/MSD/CP-84938; CONF-951135-29. Argonne National Lab.(ANL), Argonne, IL (United States), 1995.
[2] Latib, Muhammad Azamuddin, and Natrah Kamaruzaman. "Simulation Study on the Heat Performance of Different Nanofluids for Rotating Detonation Engine Cooling." *Journal of Advanced Research in Micro and Nano Engineering* 5, no. 1 (2021): 1-8.
[3] Esfe, Mohammad Hemmat, Ali Akbar Abbasian Arani, Mohammad Rezaie, Wei-Mon Yan, and Arash Karimipour. "Experimental determination of thermal conductivity and dynamic viscosity of Ag–MgO/water hybrid nanofluid." *International Communications in Heat and Mass Transfer* 66 (2015): 189-195. https://doi.org/10.1016/j.icheatmasstransfer.2015.06.003
[4] Harandi, Saeed Sarbolookzadeh, Arash Karimipour, Masoud Afrand, Mohammad Akbari, and Annunziata D'Orazio. "An experimental study on thermal conductivity of F-MWCNTs–Fe3O4/EG hybrid nanofluid: effects of temperature and concentration." *International Communications in Heat and Mass Transfer* 76 (2016): 171-177. https://doi.org/10.1016/j.icheatmasstransfer.2016.05.029
[5] Jahan, Sultana, M. Ferdows, M. D. Shamshuddin, and Khairy Zaimi. "Effects of Solar Radiation and Viscous Dissipation on Mixed Convective Non-Isothermal Hybrid Nanofluid over Moving Thin Needle." *Journal of Advanced Research in Micro and Nano Engineering* 3, no. 1 (2021): 1-11.
[6] Harun, Muhammad Arif, Nor Azwadi Che Sidik, Yutaka Asako, and Tan Lit Ken. "Recent Review On Preparation Method, Mixing Ratio, and Heat Transfer Application Using Hybrid Nanofluid." *Journal of Advanced Research in Fluid Mechanics and Thermal Sciences* 95, no. 1 (2022): 44-53. https://doi.org/10.37934/arfmts.95.1.4453
[7] Ali, I. R., Ammar I. Alsabery, Norhaliza Abu Bakar, and Rozaini Roslan. "Mixed Convection in a Lid-Driven Horizontal Rectangular Cavity Filled with Hybrid Nanofluid by Finite Volume Method." *Journal of Advanced Research in Fluid Mechanics and Thermal Sciences* 93, no. 1 (2022): 110-122. https://doi.org/10.37934/arfmts.93.1.110122
[8] Adnan Asghar, Teh Yuan Ying, Khairy Zaimi, Asghar. "MHD mixed convection hybrid nanofluid thermal radiation Joule heating velocity and thermal slip conditions." *Journal of Advance Research in Fluid Mechanics and Thermal Sciences* 95 (2022): 159–179. https://doi.org/10.37934/arfmts.95.2.159179
[9] Khan, A.A., Zaimi, K., Sufahani, S.F., and Ferdows, M. "MHD flow and heat transfer of double stratified/stretching sheet with chemical reaction and heat source." *Journal of Advanced Research in Applied Sciences and Engineering Technology* 21 (2020): 1–14. https://doi.org/10.37934/araset.21.1.114
[10] Ezhil, Kumaresan, Sravan Kumar Thavada, and Suresh Babu Ramakrishna. "MHD Slip Flow and Heat Transfer of Cu-Fe3O4/Ethylene Glycol-Based Hybrid Nanofluid over a Stretching Surface." (2020).
[11] Sreedevi, P., P. Sudarsana Reddy, and Ali Chamkha. "Heat and mass transfer analysis of unsteady hybrid nanofluid flow over a stretching sheet with thermal radiation." *SN Applied Sciences* 2, no. 7 (2020): 1-15. https://doi.org/10.1007/s42452-020-3011-x
[12] Takabi, Behrouz, and Saeed Salehi. "Augmentation of the heat transfer performance of a sinusoidal corrugated enclosure by employing hybrid nanofluid." *Advances in Mechanical Engineering* 6 (2014): 147059. https://doi.org/10.1155/2014/147059
[13] Hussain, S., Sameh E. Ahmed, and T. Akbar. "Entropy generation analysis in MHD mixed convection of hybrid nanofluid in an open cavity with a horizontal channel containing an adiabatic obstacle." *International Journal of Heat and Mass Transfer* 114 (2017): 1054-1066. https://doi.org/10.1016/j.ijheatmasstransfer.2017.06.135
[14] Khashi'ie, Najiyah Safwa, Norihan Md Arifin, and Ioan Pop. "Magnetohydrodynamics (MHD) boundary layer flow of hybrid nanofluid over a moving plate with Joule heating." *Alexandria Engineering Journal* 61, no. 3 (2022): 1938-1945. https://doi.org/10.1016/j.aej.2021.07.032

[15] Aaiza, Gul, Ilyas Khan, and Sharidan Shafie. "Energy transfer in mixed convection MHD flow of nanofluid containing different shapes of nanoparticles in a channel filled with saturated porous medium." *Nanoscale Research Letters* 10, no. 1 (2015): 1-14. https://doi.org/10.1186/s11671-015-1144-4

[16] Fakour, M., D. D. Ganji, and M. Abbasi. "Scrutiny of underdeveloped nanofluid MHD flow and heat conduction in a channel with porous walls." *Case Studies in Thermal Engineering* 4 (2014): 202-214. https://doi.org/10.1016/j.csite.2014.10.003

[17] Gholinia, M., S. Gholinia, Kh Hosseinzadeh, and D. D. Ganji. "Investigation on ethylene glycol nano fluid flow over a vertical permeable circular cylinder under effect of magnetic field." *Results in Physics* 9 (2018): 1525-1533. https://doi.org/10.1016/j.rinp.2018.04.070

[18] Yashkun, Ubaidullah, Khairy Zaimi, Nor Ashikin Abu Bakar, Anuar Ishak, and Ioan Pop. "MHD hybrid nanofluid flow over a permeable stretching/shrinking sheet with thermal radiation effect." *International Journal of Numerical Methods for Heat & Fluid Flow* (2020). https://doi.org/10.1108/HFF-02-2020-0083

[19] Merkin, J. H. "On dual solutions occurring in mixed convection in a porous medium." *Journal of engineering Mathematics* 20, no. 2 (1986): 171-179. https://doi.org/10.1007/BF00042775

[20] Weidman, P. D., D. G. Kubitschek, and A. M. J. Davis. "The effect of transpiration on self-similar boundary layer flow over moving surfaces." *International journal of engineering science* 44, no. 11-12 (2006): 730-737. https://doi.org/10.1016/j.ijengsci.2006.04.005

[21] Harris, S. D., D. B. Ingham, and I. Pop. "Mixed convection boundary-layer flow near the stagnation point on a vertical surface in a porous medium: Brinkman model with slip." *Transport in Porous Media* 77, no. 2 (2009): 267-285. https://doi.org/10.1007/s11242-008-9309-6

[22] Mukhopadhyay, Swati. "Slip effects on MHD boundary layer flow over an exponentially stretching sheet with suction/blowing and thermal radiation." *Ain Shams Engineering Journal* 4, no. 3 (2013): 485-491. https://doi.org/10.1016/j.asej.2012.10.007

[23] Thirupathi, Gurrala, Kamatam Govardhan, and Ganji Narender. "Radiative Magnetohydrodynamics Casson Nanofluid Flow and Heat and Mass Transfer past on Nonlinear Stretching Surface." *Journal of Advanced Research in Numerical Heat Transfer* 6, no. 1 (2021): 1-21. https://doi.org/10.3762/bxiv.2021.65.v1